

Disclaimer:

The contents of this report reflect the views of the authors, who are responsible for the facts and the accuracy of the information presented herein. This document is disseminated in the interest of information exchange. The report is funded, partially or entirely, under 69A3552348333 from the U.S. Department of Transportation's University Transportation Centers Program. The U.S. Government assumes no liability for the contents or use thereof.



TRANS-IPIC

TRANSPORTATION INFRASTRUCTURE
PRECAST INNOVATION CENTER

Transportation Infrastructure Precast Innovation Center

(TRANS-IPIC)

University Transportation Center (UTC)

*Bio-Inspired Solutions for Jersey and Road Noise Barriers: Exploring 3D
Printing as Alternative Precast Technology*

PU-23-RP-03

FINAL REPORT

Submitted by:

Pablo Zavattieri¹(zavattie@purdue.edu)

Jan Olek¹(olek@purdue.edu),

Jeff Youngblood²(jpyoungb@purdue.edu),

¹*Lyles School of Civil Engineering, Purdue University*

²*School of Materials Engineering, Purdue University*

Collaborators / Partners:

Terran Robotics

Sperra

Submitted to:

TRANS-IPIC UTC

University of Illinois Urbana-Champaign

Urbana, IL

Executive Summary

This report provides an overview of the mechanical performance of 3D-printed concrete elements incorporating bio-inspired architectural designs, including Bouligand and sinusoidal helicoidal patterns, and explores their potential applications in roadside barriers. The study evaluated the mechanical performance of these architected materials using both quasi-static tests and dynamic impact tests conducted with a drop tower. The results demonstrate that incorporating these innovative architectures into 3D-printed concrete elements significantly enhances compressive strength and energy absorption. Under quasi-static compressive testing, the 3D-printed element with sinusoidal helicoidal architecture exhibited a 53.6% and 13.5% increase in compressive strength compared to regular 3D-printed and cast samples, respectively. During drop tower impact testing, the sinusoidal Bouligand and Bouligand samples exceeded the peak load of the cast sample by 68.6% and 45.4%, respectively, and surpassed their absorbed impact energy by 49.2% and 54.6%. The mechanical test results highlight the superior compressive strength and impact resistance of 3D-printed elements featuring these architected materials, making them ideal for modern roadside barriers. As electric vehicles (EVs), which are heavier than traditional gasoline-powered vehicles, become more prevalent, barriers designed for lighter gasoline vehicles often fail to adequately contain these heavier EVs, leading to catastrophic failures during collisions. **Mick Syslo, Deputy Director at the Nebraska Department of Transportation, noted that "thousands of miles" of barriers may need to be replaced to meet evolving safety requirements due to the EVs.** The bio-inspired architected materials investigated in this research demonstrate a remarkable ability to prevent fatal crack development and maintain structural integrity. This is especially important as barriers must manage the greater forces generated by heavy EVs, preventing them from rebounding into traffic or penetrating the barrier.

Additionally, we explored hybrid 3D printing of two materials. For instance, we demonstrated that cement-silicone hybrid 3D-printed elements offer unique advantages, including enhanced energy dissipation and deformation capacity. Silicone, with its inherent flexibility and elasticity, increases deflection and helps prevent catastrophic failure. When paired with cementitious materials, which provide rigidity and load-bearing capacity, the composite material exhibits enhanced energy absorption capacity, making it ideal for applications such as roadside barriers. This first year, we also examined the acoustic performance of a shape-shifting noise barrier designed to mitigate noise at different frequencies by dynamically adjusting the configuration of embedded elements with phononic crystal-inspired designs. The findings indicate improvements in noise mitigation, demonstrating the potential of the application of this technology for transportation infrastructure. **Four patents** have been filed for this project. We plan to contact potential industry partners, including the **National Precast Concrete Association, Trinity Highway Products, Lindsay Corporation, and Traffix Devices.**, to assess their interest in developing this new barrier type. We delivered eight presentations at conferences and UTC webinars, prepared two papers, launched a new course (CE 497) on 3D printing for infrastructure in Spring 2024, and hosted high school students from various Purdue programs for lectures and demonstrations on 3D printing and mechanical testing.

Table of Contents

1. Problem statement	5
2. Research plan/task	6
3. Main results	6
Task 1: Fabrication	6
Task 1.1 Design and fabricate a 3D printing system for cement-based materials	6
Task 1.2 Design a system for polymer-cement 3D printing	7
Task 2: Architected material designs	8
Task 2.1 Bio-inspired architected material designs for energy absorption	8
Task 2.2 Reconfigurable acoustic material design for noise mitigation	9
Task 3: Material characterization and testing	10
Task 3.1 Quasi-static and drop tower impact test	10
Task 3.2 Noise mitigation test	15
4. Educational outreach activities	18
5. Technology transfer actions	18
6. Publications and Presentations	18
7. Reference	19

1. Problem statement

The continuous improvement of transportation infrastructure is essential for ensuring the safety of road users and maintaining the efficiency of the transportation network. A critical element of this enhancement is the incorporation of impact-resistant structures in the construction and retrofitting of infrastructure components, such as roadside barriers. Recently, the growing prevalence of electric vehicles (EVs) has introduced significant challenges to the performance and safety of these barriers. Due to their heavier weight (mainly from batteries), EVs generate increased impact forces that conventional barriers are not designed to withstand [1–5]. Recent crash tests have shown that current barriers, which are optimized for lighter gasoline-powered vehicles, often fail to contain heavier EVs, leading to catastrophic consequences [1–5]. For instance, as shown in Fig. 1, a 7,000-pound Rivian R1T truck crushed and tore through concrete barriers commonly used as freeway median barriers or to shield highway construction workers from ongoing traffic, with minimal deceleration, posing significant risks to both passengers and infrastructure [1, 2]. This issue is compounded by the fact that EVs can weigh 20% to 50% more than traditional vehicles, drastically increasing the energy transferred during collisions [1, 2].

As EVs gain popularity, improving the energy absorption capacity and impact resistance of roadside barriers is crucial. Developing more robust barrier designs that can manage these heavier loads is vital not only for public safety but also for preserving transportation infrastructures, which are not currently built to accommodate such heavy vehicles. Collaborative research efforts, such as those led by the Midwest Roadside Safety Facility and the U.S. Army Corps of Engineers, address these pressing issues by developing next-generation barriers that can handle the higher impacts from modern vehicles, ensuring future roadway safety in a rapidly evolving landscape. In our project, we aim to leverage 3D printing technology and bio-inspired design principles to enhance the energy absorption capacity of concrete barriers, thereby improving their effectiveness in ensuring future roadway safety. We have demonstrated the ability to make concrete both stronger and more energy-absorbing under impact conditions— a breakthrough achieved by combining clever architectures inspired by extreme animals in nature with 3D concrete printing technology.

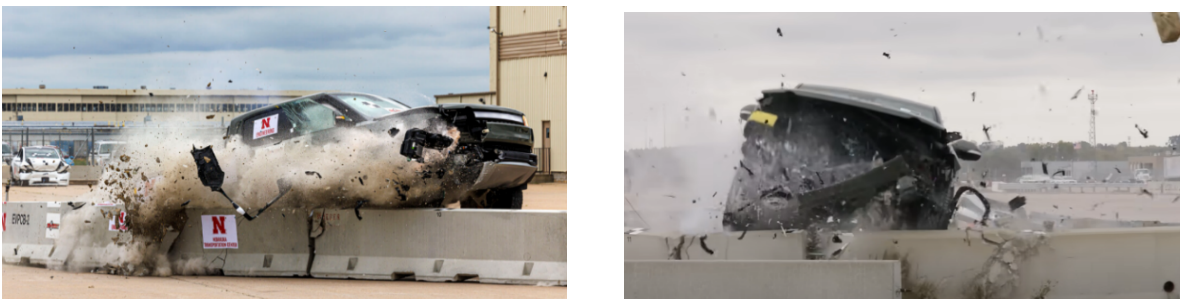


Fig. 1. A 7,000-pound Rivian R1T truck crushed and tore through concrete barriers commonly used as freeway median barriers or to shield highway construction workers from ongoing traffic, with minimal deceleration, posing significant risks to both passengers and infrastructure [1, 2].

2. Research plan/tasks

Task 1: Fabrication

Task 1.1: Develop a specialized printing head for accurate deposition of concrete in a layer-by-layer fashion, optimizing for strength, durability, and high-strength structures for both LALS and LSRA printers.

Task 1.2: Design and fabricate a printing head for extruding polymeric material, strategically integrating it into the biomimetic Jersey barrier design to create energy-absorbing weak interfaces. During our first year, we will implement this in our LALS printer and will plan our implementation for the LSRA printer in subsequent years.

Task 2: Architected Material Designs

Task 2.1: Develop biomimetic architectures inspired by nature to optimize energy dissipation in the Jersey barriers, incorporating weak interfaces, cellular structures, and geometric patterns using both LALS and LSRA printers.

Task 2.2: Study and develop architected materials specifically tailored for acoustic barriers, aiming to mitigate road/traffic noise and the use of shape-shifting materials for reconfigurable barriers that can adapt to different noise patterns and frequency spectra variations.

Task 3: Material Characterization and Testing

Tasks 3.1: Conduct comprehensive material characterization and testing of the 3D printed biomimetic Jersey barriers, including mechanical tests to assess strength, deformation behavior, and energy absorption capacity under quasi-static conditions. Additionally, perform dynamic (drop-tower) impact tests to evaluate performance in simulated collision scenarios.

Tasks 3.2: Evaluate efficiency of reconfigurable traffic noise barriers based on shape-shifting materials using low-cost DIY impedance tube testing to measure sound absorption and transmission loss of the barriers in a controlled environment.

3. Main results

Task 1: Fabrication

Task 1.1 Design and fabricate a 3D printing system for cement-based materials

In Task 1.1, a comprehensive large-scale 3D concrete printing system was developed. The system includes an ABB robotic arm (ABB 6700), a high-pressure mortar pump (M-Tech Duo mix P20), and a high-performance extruder designed by the research group (Fig. 2). A notable achievement in this task was the successful fabrication of a curved wall section using the 3D printing (3DP) system. The curved wall, with a total length of 9.4' and a height of 3', was designed for incorporation into a 3D-printed earth house in Bloomington, Indiana, showcasing the practical application of this advanced technology. A 1-inch nozzle was used for the print, with the layer height set at 10mm, yielding a total of 90 layers. Quikrete 3D printing mixture was used to expedite the system testing phase.

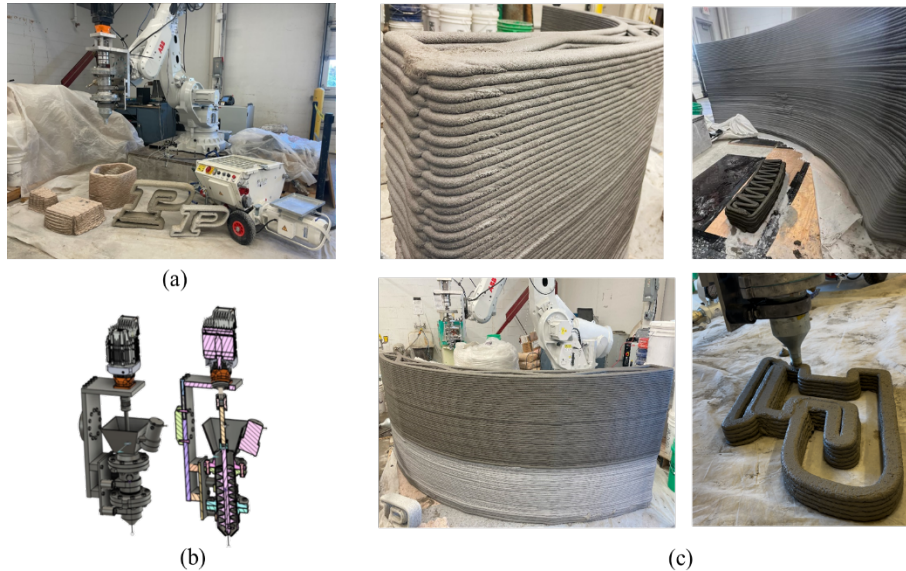


Fig. 2. (a) large-scale 3D printing system including robotic arm, pump, and extruder (b) Design of the extruder (c) specimens fabricated with the 3DP system.

Task 1.2 Design a system for polymer-cement 3D printing

In task 1.2, we aimed to explore the fabrication method for the 3D printing of cement paste and polymer materials to create functional composite materials. This involved designing and adding silicon delivery printing head (syringe) to the small-scale printer (Fig. 3 (a) and (b)). The silicone used exhibited suitable rheological properties for extrusion, though there were some challenges with its buildability. To address this issue, we designed a toolpath geometry that enabled the installation of a silicone layer between cement paste filaments while allowing for the deposition of a second layer of cement paste without causing the sample to collapse (Fig. 3 (a) and (b)). The cement paste-silicone composite material was designed to create hard-soft material interfaces to optimize energy absorption capacity. Mechanical performance of this composite was evaluated through three-point bending flexural tests. As shown in Fig. 3(c), the 3D-printed cement paste samples exhibited brittle failure upon reaching peak load, while the composite samples, consisting of both, cement paste and silicone, displayed multiple small load drops in the load-displacement curves. This behavior suggests the formation of multiple cracks rather than a single crack leading to catastrophic failure. Fig. 3 (d) presents the fracture pattern of the composite sample, which shows multiple cracks formation as well as strong stretch-recovery behavior due to the presence of silicone. The results demonstrate that by combining polymer with cement paste, a highly stretchable composite with enhanced energy absorption capacity can be created, outperforming samples prepared from paste with no silicon addition.

This achievement is significant for the continuation of the project. Future efforts should focus on enhancing the rheological properties of the polymer, possibly through polymer synthesis or increasing solid content. The ability to print both polymer and cement paste opens opportunities to optimize energy absorption in materials for roadside barriers. In nature, hard-soft interfaces are used to dissipate energy effectively. For example, the integration of flexible polymeric nanofibers with rigid mineral components results in a periodic variation in stiffness [6]. When this feature is combined with the helicoidal (Bouligand) architecture, it promotes crack twisting, thereby increasing the material's ability to resist fracture and absorb more energy [6]. Now, with the

capability to 3D print two materials, we could incorporate soft polymers into cement paste during the printing process, mimicking nature’s hard-soft material combinations. This could further optimize energy absorption properties. Furthermore, 3D printing with polymer-cement materials offers the potential to develop phase-transforming cellular materials with reconfigurable properties for the reconfigurable noise barrier proposed in this project. These materials could function as actuators, dynamically adjusting the periodic arrangement of phononic crystal structures to optimize noise mitigation based on varying conditions such as vehicle type, speed, and construction activities.

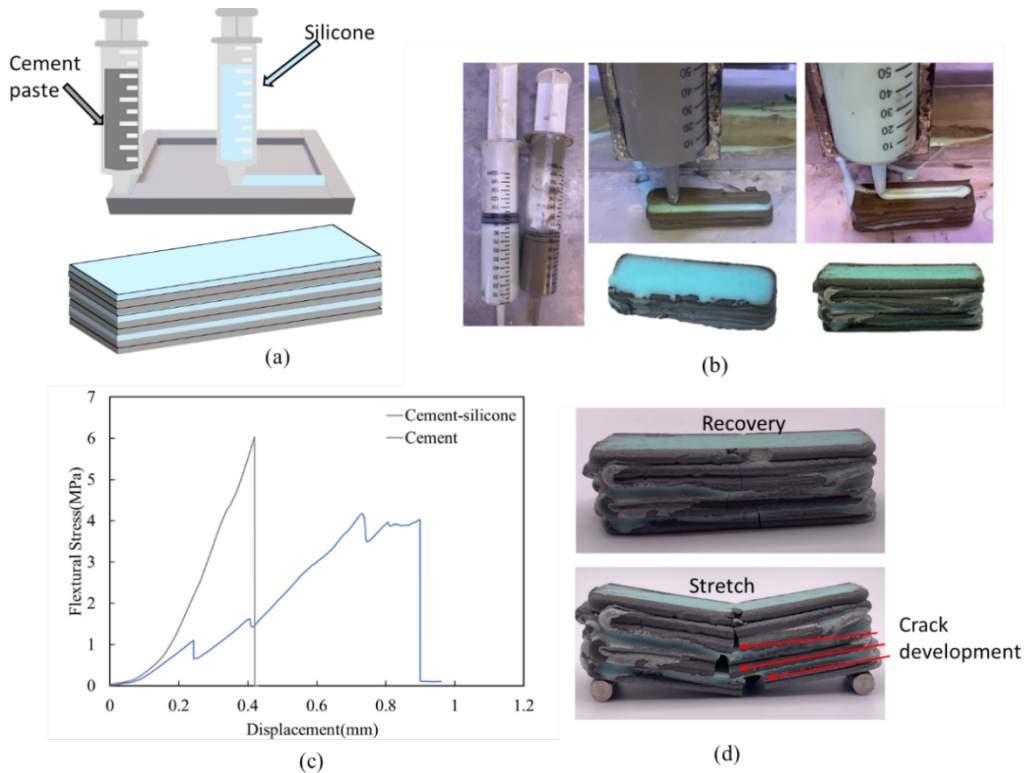


Fig. 3. (a) Schematic illustrating 3D printing of cement paste and silicone using syringe extrusion. (b) Examples of cement-silicone composite samples fabricated by small scale 3D printer(c) Load-displacement curves from the three-point bending test for 3D-printed samples: cement paste only and cement paste-silicone composite (d) fractured sample showing high stretch recovery behavior

Task 2: Architected material designs

Task 2.1 Bio-inspired architected material designs for energy absorption

In **task 2.1** we identified two biomimetic architectures inspired by dactyl club of mantis shrimp to optimize energy dissipation in the Jersey barriers. Mantis shrimp is a remarkable creature capable of delivering powerful strikes to its shelled prey [6] [7] [8]. These dactyl club exhibit peak striking speeds of approximately 20 meters per second and can generate forces of around 700 Newtons [6] [7] [8]. What makes the dactyl club especially impressive is its capacity to withstand the immense forces encountered during this predation interaction [8]. The Bouligand and sinusoidal helicoidal architectures (Fig. 4) within the dactyl club play a pivotal role in providing energy dissipation, load-bearing capabilities, and damage tolerance [6]. These characteristics are attributed to their

helicoidal arrangement and the presence of interfaces [9]. The strong anisotropy inherent in 3D-printed fiber-reinforced mortar, coupled with the presence of interfaces in the 3D-printed elements, suggests the potential for superior energy absorption capacity when incorporating Bouligand and sinusoidal helicoidal architectures. The results of this research hold promise for potential applications in energy-absorbing materials, such as in the design of precast Jersey barrier.

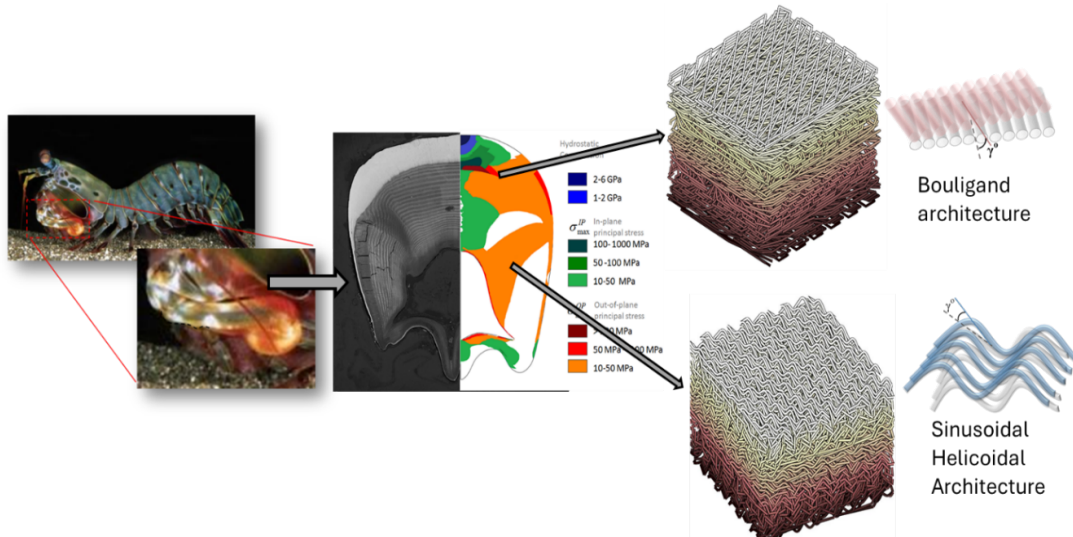


Fig. 4. Architected material design with Bouligand architecture and sinusoidal helicoidal architecture inspired by dactyl club of mantis shrimp

Task 2.2 Reconfigurable acoustic material design for noise mitigation

In Task 2.2, we studied and developed architected materials specifically designed for acoustic barriers, with the goal of mitigating road and traffic noise. We explored the use of shape-shifting materials for reconfigurable barriers that can adapt to varying noise patterns and frequency spectra. In this study, we developed an adaptive acoustic metamaterial by integrating phononic (or sonic) crystals with phase-transforming cellular materials (PXCMS) (Fig. 5). PXCMS are innovative materials that can be designed with a bistable configuration [10], allowing them to reconfigure the periodic arrangement of phononic crystals dynamically. Fig. 5 (c) and (d) present a schematic of the structure featuring hexagonal lattice patterns in both open and closed configurations. This reconfigurability is essential because it enables the periodic structure of the phononic crystals to adapt to varying traffic noise frequencies, enhancing noise mitigation across a broad spectrum. 3DP cement paste samples with triangle geometry were used as the column elements in the phononic crystals. As illustrated in Fig. 5 (c) and (d), using PXCMS as an actuator allows the arrangement of phononic crystals to be actively modified. The spacing between the columns of these crystals is a key factor that determines the specific frequencies at which noise is mitigated. Adjusting these distances can alter the spectral properties of the bandgaps, enabling the metamaterial to respond effectively to changes in noise frequency. Research by Thota et al. (2017) has demonstrated that compact hexagonal patterns are particularly effective at mitigating high-frequency noise compared to more loosely arranged hexagonal patterns [11]. This finding underscores the potential

of reconfigurable acoustic metamaterials in applications where adaptive noise control is crucial, such as in urban environments affected by fluctuating traffic noise levels.

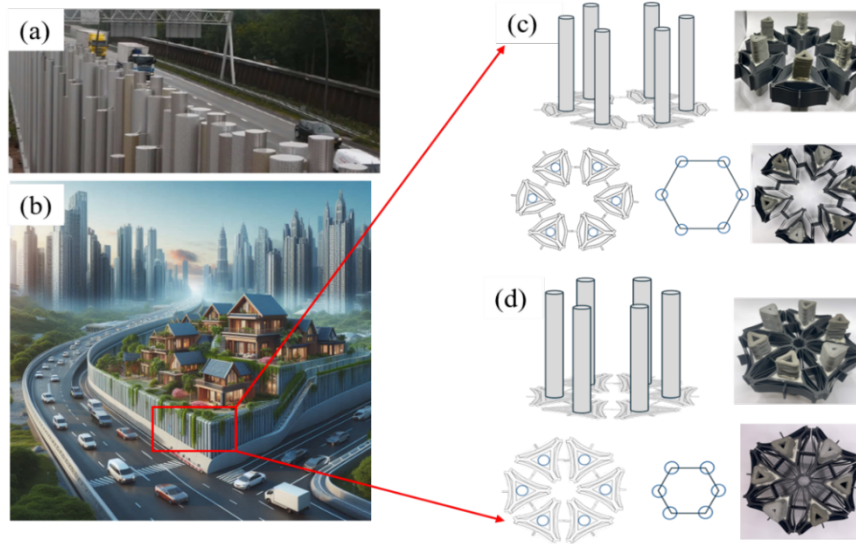


Fig. 5. (a) Periodic pipe noise barrier on a highway [7]; (b) illustration of the phononic/sonic crystal noise barrier; (c) schematic and specimens developed for reconfigurable phononic/sonic crystals integrated with phase-transforming cellular materials (PXCMS), featuring hexagonal lattice patterns in two configurations: (c) open configuration and (d) closed configuration.

Task 3: Material characterization and testing

Task 3.1 Quasi-static and drop tower impact test

In task 3.1, we evaluated the mechanical performance of the 3D printed elements under quasi-statics and impact loading conditions. In order to design 3D printed concrete with the Bouligand and sinusoidal helicoidal architectures and use these designs for transportation infrastructure such as roadside barriers, the first step is to evaluate the anisotropic properties due to the presence of the interfaces in the 3D printed sample. The interfacial properties will be used for the future design of the architected materials for transportation infrastructure applications. In this project, we evaluated the mechanical performance of the 3D printed concrete sample and compared it with the cast samples under compressive and flexural loads. The samples were tested in various directions to assess the anisotropic properties of the 3D printed specimens, which arise from the presence of the interfaces. Mortar mixtures with 5mm steel fibers were printed with our small-scale printer for this study.

As depicted in Fig. 6, an investigation of anisotropic behavior under flexural test was conducted on samples fabricated with filament orientations of 0 and 90 degrees, along with steel fiber volume fractions of 1%, 0.5%, and 0%. The flexural strength of the 0-degree sample with 1% and 0.5% steel fiber was 45.4% and 20.2% higher, respectively, compared to the sample without fiber. In contrast, the 90-degree samples show no notable improvement in flexural strength upon the addition of fibers. Moreover, the flexural strength of the 0-degree sample with 1% fiber was 156.2% greater than that of the 90-

degree sample with 1% fiber, while the flexural strength of the 0-degree sample without fiber was 96.9% higher than that of the 90-degree sample without fiber.

These findings demonstrate a notable improvement in flexural strength upon the addition of fibers in the 0-degree sample, while the 90-degree sample exhibits no substantial enhancement, thus highlighting a strong anisotropy present in the 3DP samples. This disparity in strength improvement can be attributed to the tendency of fibers to align with the printing direction during the 3D printing process. These anisotropic properties, and the existing interfaces, will be leveraged to design novel architected materials with unique functionalities for transportation infrastructure applications.

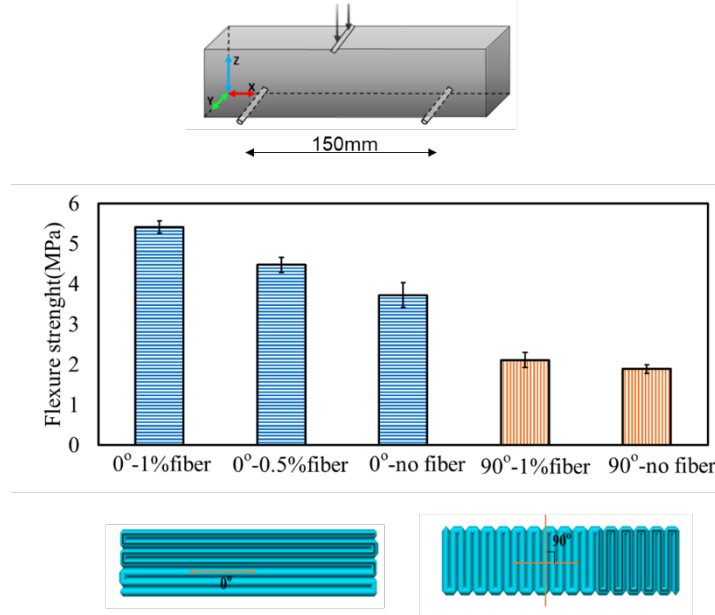


Fig. 6. Three-day flexural strength under three-point bending test for samples with different filament orientations and fiber volume fractions.

Fig. 7 presents the result of the compressive tests of the 3D printed element featuring bio-inspired architectures. A comparison is made between the compressive strength and work of failure (WOF) of samples with different filament architectures. WOF is computed as the area under the load-displacement curve up to a specified level of damage, representing the energy required to cause the failure of the sample. In this study, WOF was estimated by calculating the area under the load-displacement curve after reductions of 0%, 20%, and 40% in the peak load. With the incorporation of Bouligand architecture, the compressive strength of Bu-10 and Bu-5 samples (representing samples with 10- and 5-degree pitch angles) exceeded that of the regular 3DP sample loaded in Z-direction (see Fig. 6) by 22.5% and 18.4%, respectively, while remaining 8.6% and 14.4% lower than that of the cast counterparts. Additionally, the 40% Drop WOF of Bu-10 and Bu-5 samples exhibited strength levels similar to the cast samples and were 142.3% and 126.8% larger than that of the Z-direction loaded regular 3DP sample. With the incorporation of sinusoidal helicoidal architecture, both the compressive strength and WOF experienced significant enhancements. Specifically, the compressive strength of SinHeli-10 and SinHeli-5 samples (representing samples with 10- and 5-degree pitch angle) exceeded

that of the Z-direction loaded regular 3DP sample by 53.6% and 31.5%, respectively. Additionally, the 40% Drop WOF of SinHeli-10 and SinHeli-5 samples exhibited increases of 216% and 214% compared to the regular 3DP sample. When compared to the cast samples, SinHeli-10 exhibited a 13.5% higher compressive strength. Furthermore, the average 40% Drop WOF of SinHeli-10 was 35% greater than that of the cast counterparts.

The comparison of the results highlights the ability of Bouligand and sinusoidal helicoidal architectures to enhance compressive strength, increase work of failure and energy dissipation. It is evident that filament architecture plays a pivotal role in enhancing mechanical responses. This is particularly noteworthy for Bouligand and sinusoidal helicoidal designs, due to their ability to utilize twist crack mechanisms along the interface, facilitating the spread of damage and enhancing energy dissipation. Moreover, in the case of the sinusoidal helicoidal architecture, fibers are likely to align with the sinusoidal shape, which results in distinct mechanical behavior under compressive load. This alignment enhances the material's ability to resist deformation and improves overall mechanical performance.

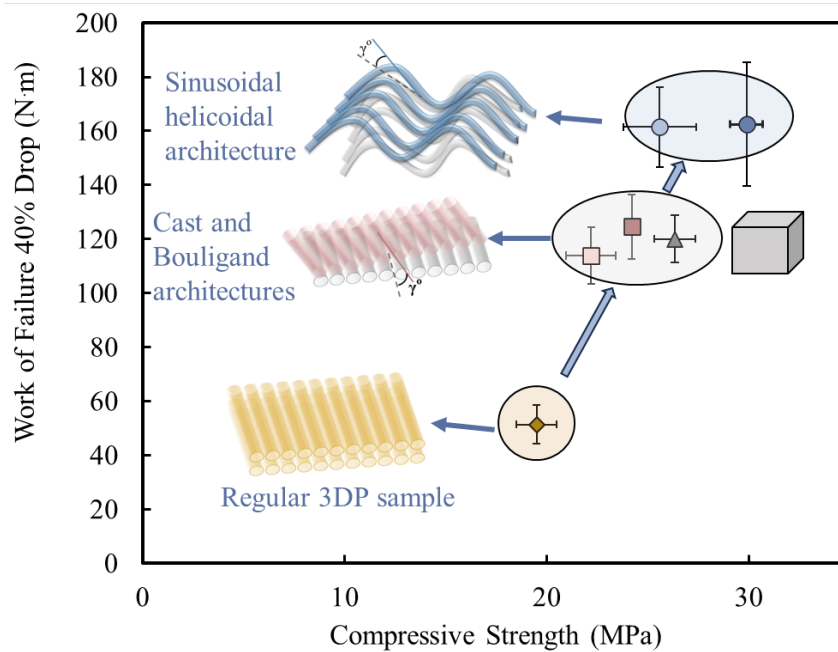


Fig. 7. Compressive strength comparison between cast samples, 3DP sample with sinusoidal helicoidal, Bouligand architecture and regular filament configuration.

Most significantly, this study demonstrated that the sinusoidal helicoidal architecture statistically improved compressive strength and work of failure compared to the cast samples. Given the critical need for optimal mechanical properties in transportation infrastructure, this enhanced performance can directly contribute to the improvement of transportation infrastructure systems.

In this task, we also present the result of dynamic (drop-tower) impact tests to evaluate performance of the bio-inspired architectures under impact loading condition. Five sample

configurations were tested, including cast mortar with and without fibers, and 3DP samples with Bouligand, sinusoidal Bouligand, and regular straight printing configurations. The tests were conducted with two impact energies: 56.7J and 70.9J.

Fig. 8 presents the load-deflection results and fracture patterns from the drop tower impact tests for cast samples (with and without fibers) and 3D-printed samples using Bouligand, sinusoidal Bouligand, and regular straight filament configurations, subjected to impact energies of (a) 56.7J (drop height of 0.8m) and (b) 70.9J (drop height of 1m). The force-displacement curves highlight the differing abilities of these configurations to respond to dynamic impact loads and absorb energy. The higher peak loads and delayed decline in the curves for the sinusoidal Bouligand and Bouligand samples indicate their enhanced impact resistance at both energy levels. At a drop height of 0.8m (Fig. 8 (a)), the sinusoidal Bouligand sample achieved the highest peak force (14,666.4N) and absorbed 56.6J of energy, while the Bouligand sample reached a peak force of 9,968.5N, absorbing 53.6J of energy. The sinusoidal Bouligand sample demonstrated the highest peak load of all samples and exhibited similar energy absorption to the Bouligand sample. The sinusoidal Bouligand design outperformed the other configurations, with a peak load 52.4% higher than the regular 3D-printed samples and 34.8% higher than the cast samples with fibers. In comparison, its absorbed impact energy increased by 20.8% and 29.7%, respectively. Compared to the cast sample without fibers, the sinusoidal Bouligand sample showed a 98.8% increase in peak load and a 102.6% increase in absorbed impact energy.

As shown in Fig. 8 (b), at an increased impact energy of 70.9J (from a drop height of 1m), the sinusoidal Bouligand sample exhibited a peak force of 14,133.8N and absorbed 66.3J of energy. In contrast, the Bouligand sample reached a peak force of 12,192.5N, absorbing 68.7J of energy. The cast sample with fibers exhibited a peak load of 8,383.8N and absorbed 44.5J of impact energy. The sinusoidal Bouligand and Bouligand samples surpassed the peak load of the cast sample by 68.6% and 45.4%, respectively, and exceeded their absorbed impact energy by 49.2% and 54.6%. Compared to the results at the drop height of 0.8m, the energy absorbed by the sinusoidal Bouligand and Bouligand samples increased, while the energy absorbed by the cast sample remained similar due to the fatal damage it sustained.

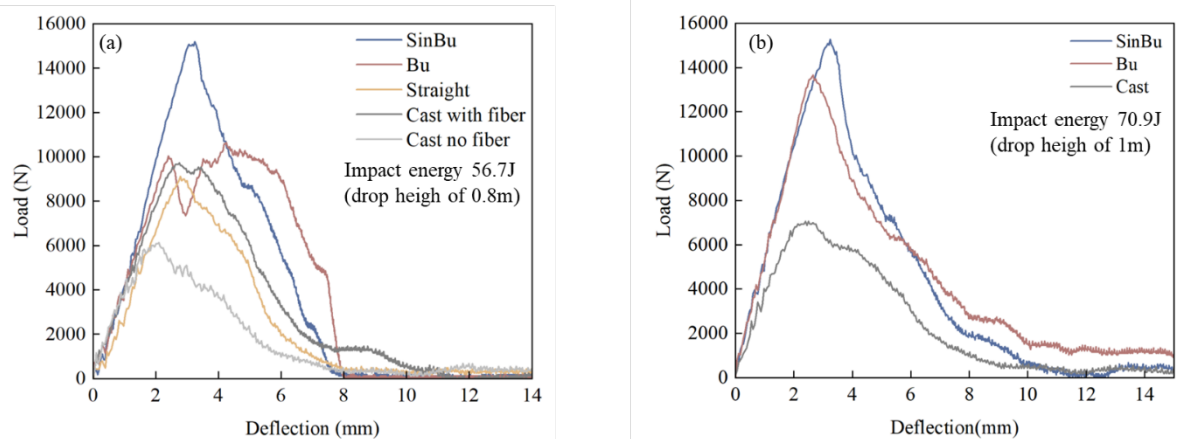


Fig. 8. Load-deflection results and fracture patterns from the drop tower impact test for cast samples (with and without fiber) and 3D-printed samples with Bouligand, sinusoidal Bouligand, and regular straight filament configurations, subjected to impact energies of (a) 56.7J (drop height of 0.8m) and (b) 70.9J (drop height of 1m).

Fig. 9 (a) compares the fracture patterns and shows the Ashby plot, illustrating the average peak impact load and absorbed energy for different samples under an impact energy of 56.7J (drop height of 0.8m). It is evident that the sinusoidal Bouligand sample exhibited the highest peak load and absorbed highest amount of energy compared to the other configurations. The Bouligand sample shows a slightly lower peak load but similar level of absorbed energy compared to the sinusoidal Bouligand. Notably, both the sinusoidal Bouligand and Bouligand samples outperform the cast samples. As seen in the fracture pattern images, these designs demonstrate excellent resistance to crack propagation, effectively maintaining their structural integrity under impact conditions.

In contrast, the cast samples (with and without fibers) and the regular 3D-printed samples suffer significant structural damage, failing to absorb the full impact energy and exhibiting severe failure. These results underscore the superior impact resistance of the sinusoidal Bouligand and Bouligand structures. Fig. 9 (b) compares the fracture patterns and shows the Ashby plot, showcasing the average peak impact load and absorbed energy for different samples under two impact energy levels (56.7J and 70.9J). Both the sinusoidal Bouligand and Bouligand samples exhibit increased energy absorption as the imposed energy rises. These designs are more effective under impact loading conditions than the cast samples, owing to their ability to prevent fatal crack development and maintain structural integrity. In contrast, the cast samples fail to absorb higher impact energy due to the extensive damage they sustain under both conditions.

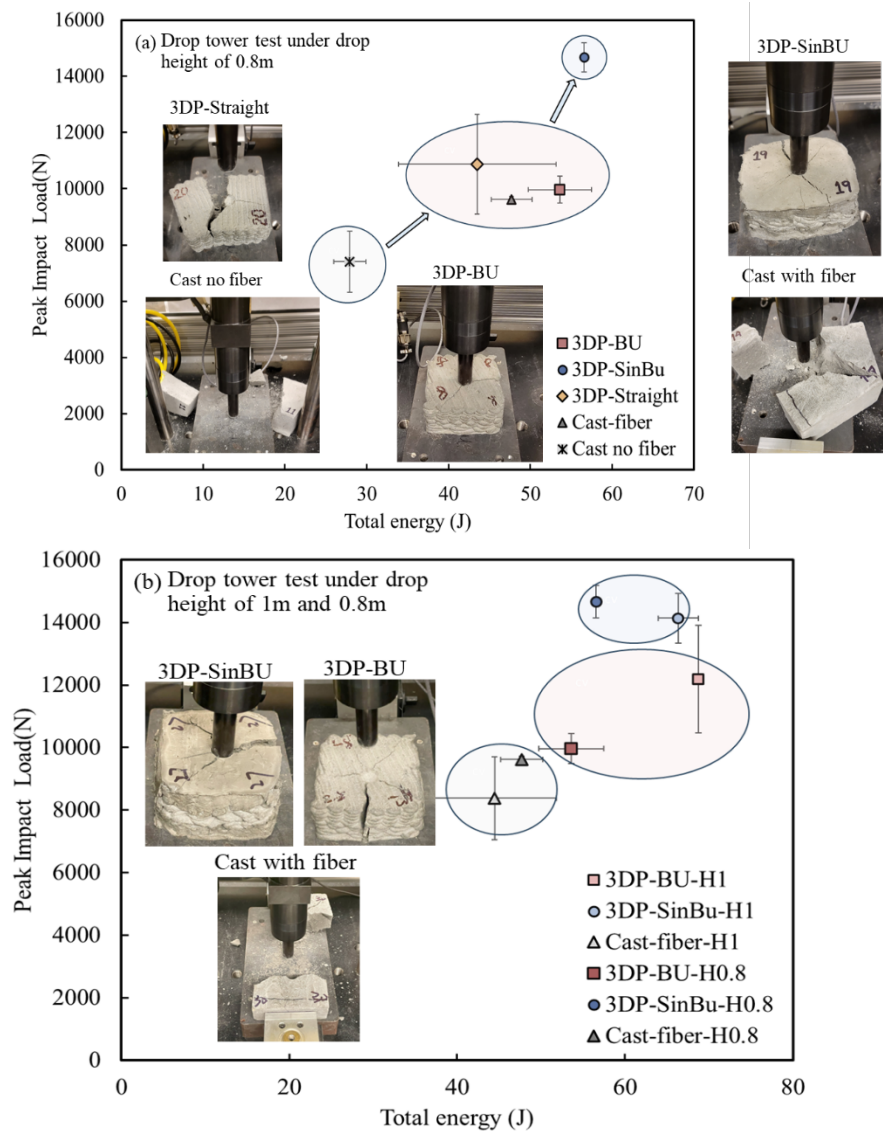


Fig. 9. Results of drop tower impact tests: (a) Comparison of fracture patterns and Ashby plot showing the average peak impact load and absorbed energy for different samples under two impact energies: 56.7J (drop height of 0.8m) and 70.9J (drop height of 1m); (b) Comparison of peak impact load and absorbed energy for different samples under an impact energy of 56.7J (drop height of 0.8m)

Task 3.2 Noise mitigation test

In task 3.2, we measured the noise absorption ratio of a barrier under two different shape configurations in a noise-isolated environment. The barrier is a shape-shifting structure, and by altering its shape, the distance between the embedded phononic crystals changes. The objective was to examine how these configuration changes affects the barrier's ability to mitigate sound across different frequencies.

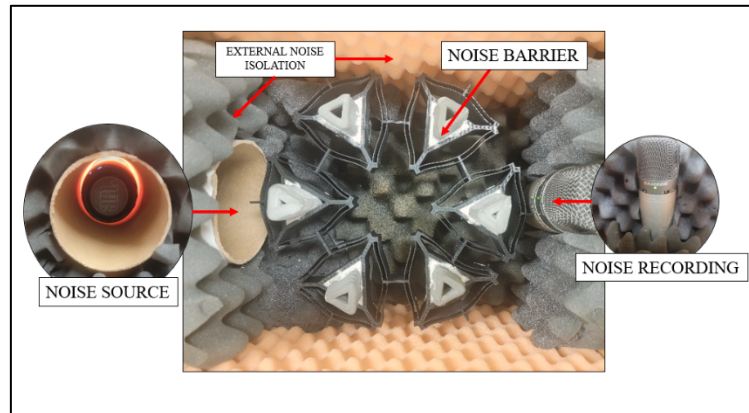


Fig. 10. Noise absorption experiment set up

A MATLAB code, capable of generating sound at various frequencies, was developed to facilitate this experiment. The generated frequencies were transmitted through a speaker positioned on one side of the barrier, and the resulting sound was recorded on the opposite side using a microphone. The root mean square (RMS) power of the original signal was compared to that of the recorded signal, and the difference was used to calculate the noise absorption ratio, using the following formula:

$$\text{Absorption Ratio} = 1 - \frac{\text{RMS of Original Signal}}{\text{RMS of Recorded Signal}}$$

By conducting the experiment with both barrier configurations, we analyzed the variation in noise absorption ratio across different frequencies, identifying which configuration provided more effective noise absorption at specific frequencies. The plot of absorption ratio vs. frequency reveals how the arrangement of phononic crystals affects sound attenuation in each configuration. The experiment was conducted using a scaled-down prototype of the proposed barrier, following the scaling method described by Thota and Wang [11]. The noise barrier depicted in Fig. 11 is a 1:7 scale model of the barrier intended for roadway use. Since the frequency range of traffic noise typically varies between 350 and 1500 Hz, the frequencies for the experiment were scaled to match this range. Consequently, the testing spectrum was set to vary from 2.5 kHz to 10.5 kHz [11].

A preliminary run of the program was performed to measure the noise absorption of the system depicted in Fig. 11 without the noise barrier inside, and the results are shown in Fig. 11 (blue trace). The figure also shows the results for the experiments conducted with the barrier set in the open configuration (red trace) and closed configuration (green trace). The frequencies tested during the experiment ranged from 2.5 kHz to 10.5 kHz, with 10 Hz increments. In a preliminary run of the experiment, peaks in the noise absorption ratio were detected at 4200 Hz and 9067 Hz, which can be interpreted as system resonance frequencies (without the barrier), where wave cancellation occurs. When the barrier was placed, these resonance frequencies were slightly altered, either increasing the absorption or shifting the peak frequencies. At 4200 Hz, the absorption ratio increased by 10.609% with the barrier in the open configuration and by 26.83% in the closed configuration. The resonance frequency at 9067 Hz shifted to 9183.8 Hz in the open

configuration and to 9772 Hz in the closed configuration, with a 10.83% decrease in the absorption ratio.

Significant changes in noise absorption were observed across the frequency spectrum when switching between configurations. The most significant change occurred at 6150 Hz, where the absorption ratio increased from 0.282 in the open configuration to 0.914 in the closed configuration. Additionally, for frequencies of 10257 Hz, the absorption ratios increased from 0.348 (open configuration) to 0.808 (close configuration). A similar effect can be observed at 3130 Hz, where the absorption ratio increased from 0.188 (open configuration) to 0.469 (closed configuration). In accordance with the previously described scale factor (based on the literature [11]), the major impacts for real-world applications (at 1:1 scale) are expected to occur at frequencies around 447.142 Hz, 878.571 Hz and 1428.571 Hz and higher. When switching from the closed to the open configuration, the highest impacts were observed at 5080 Hz, where the absorption ratio increased from 0.421 to 0.914, and at 7120 Hz, where the absorption ratio rose from 0.228 to 0.776. These frequencies correspond to 725.714 Hz and 1017.142 Hz, respectively, for 1:1 scale [11]. On the other hand, no major changes in the absorption ratio were observed. at frequencies near 2760 Hz, 3500 Hz, 3900 Hz, 5570 Hz, 6870 Hz, 7716 Hz, and 8750 Hz,

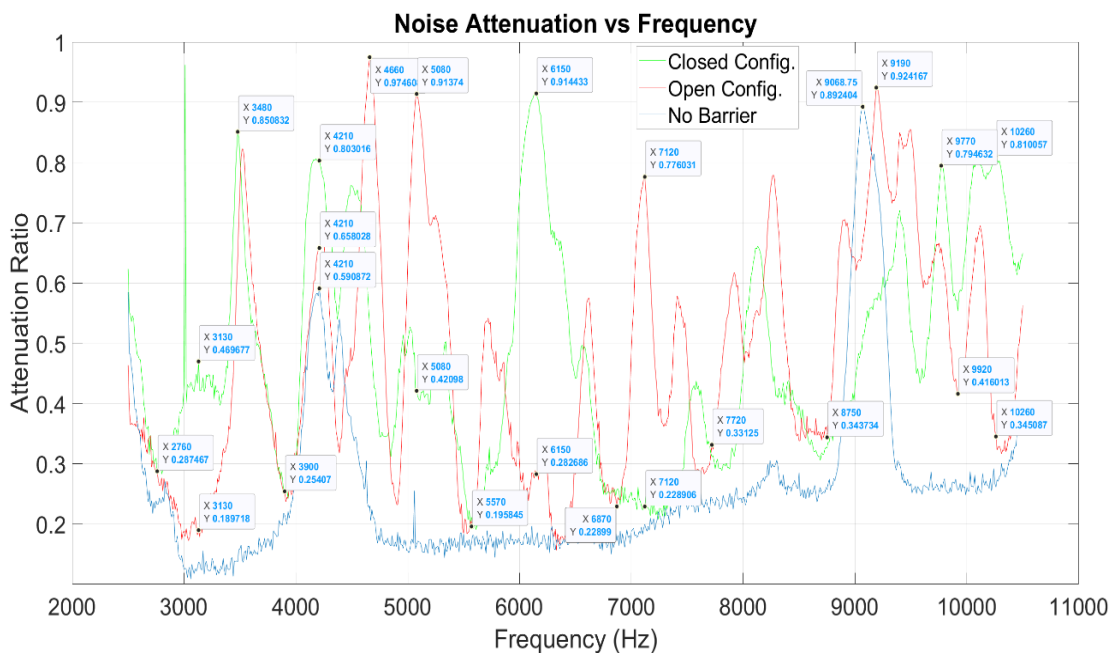


Fig. 11. Absorption Ratio – Frequency graphic for different shape-shifting barrier configurations.

These low-cost experiments demonstrated the ability to alter the barrier's working frequency intervals. However, they also highlighted the need for more advanced data analysis and filtering methods to better understand the effects of external noise and system geometry on the results. Future work will focus on increasing noise absorption across the frequency spectrum by modifying the shape-shifting lattice geometry, as well as incorporating other noise-mitigating metamaterials into the design.

4. Educational outreach activities

- In the Spring 2024 semester, the research team introduced a new three-credit undergraduate course, CE 497: 3D Printing for Infrastructure Applications. The course focuses on the principles and practical applications of 3D printing technology in concrete infrastructure.
- In August 2024, the research group hosted two cohorts of high school students as part of Purdue University's Summer College for High School Students and the Gifted Education Research and Resource Institute programs. The visit featured demonstrations with a small-scale gantry system and a large-scale robotic arm system, showcasing cutting-edge applications. Additionally, a lecture was delivered on the fundamentals of 3D printing technology for infrastructure applications, providing students with valuable insights into this innovative field.
- In the Fall 2024 semester, the research group hosted a visit for 30 high school students participating in Purdue University's Minority in Engineering Program. The visit included guided tours of various lab facilities in the School of Civil and Construction Engineering at Purdue University.

5. Technology transfer actions

Patent/Disclosure filled:

A patent for energy-absorbing roadside barriers is **available for licensing**. We plan to reach out to potential industry partners, including the **National Precast Concrete Association, Trinity Highway Products, Lindsay Corporation, Traffix Devices, and Road Systems, Inc.**, to collaborate on developing this innovative barrier type.

- Zavattieri, P. D., Youngblood, J. P., Olek, J., Wang, Y., Energy-Absorbing Roadside Barriers Using Bio-Inspired Architecture and 3D Concrete Printing.
- Zavattieri, P. D., Youngblood, J. P., Olek, J., Wang, Y., Cubillos, L. David, Novel Lightweight and Flexible Barrier for Traffic Noise Reduction.
[Novel Lightweight and Flexible Barrier for Traffic Noise Reduction | Purdue OTC](#)
- Youngblood, J. P., Olek, J., Zavattieri, P. D., Wang, Y., Douba, E. A., Low Carbon, Low-Cost Cement Mix Containing Cellulose Nano Fiber and Limestone Filler For 3D Concrete Printing.
- Zavattieri, P. D., Olek, J., Marika Santagata, Youngblood, J. P., Wang, Y., Hygrolock-reinforcement for building blocks made of earth materials.

6. Publications and Presentations

Papers under internal review

- Wang, Y., Olek, J., Zavattieri, P. D., Youngblood, J. P., Enhancing Strength and Impact Resistance of Concrete Through Biomimetic Sinusoidal Helicoidal Architectures Enabled by Additive Manufacturing.
- Wang, Y., Douba, E. A., Cubillos L. D. Olek, J., Zavattieri, P. D., Youngblood, J. P., Low Carbon and Low-Cost Cement Mix With Enhanced Rheology And Mechanical Properties For Concrete 3d Printing.

Presentations

- Y. Wang, P. Zavattieri, J. Olek, J. Youngblood, “3D Printing of Concrete with Bioinspired Design: A Study on Impact Resistance”, presented at the American Concrete Institute (ACI) Fall 24 convention, Philadelphia, PA.
- Y. Wang, P. Zavattieri, J. Olek, J. Youngblood, “Sinusoidal Helicoidal Architecture with Nonplanar Layering of Filaments in Additively Manufactured Cementitious Materials”, American Concrete Institute (ACI) Fall 24 convention, Philadelphia, PA.
- J. Olek, P. Zavattieri, J. Youngblood, Y. Wang, F. Rodriguez, R. Moini, Development of cementitious mixtures for 3D printing of elements with controlled architecture, UTC DuRe-Transp online research webinar, July 23, 2024.
- Y. Wang, A. Douba, J. Olek, J. Youngblood, P. Zavattieri “Sustainable cementitious composite containing cellulose nano fibers for concrete 3D-Printing”, American Concrete Institute (ACI) Spring 24 convention, New Orleans, LA.
- Y. Wang, P. Zavattieri, J. Olek, J. Youngblood, “Bio-inspired Sinusoidal Helicoidal Architecture in Additively Manufactured Cementitious Materials” Engineering Mechanics Institute (EMI) Conference Spring 2024, Chicago, IL
- Y. Wang, P. Zavattieri, J. Olek, J. Youngblood, “Bio-Inspired Solutions for Roadside Barriers: Exploring 3D Printing as Alternative Precast Technology”, UTC Trans-IPIC online research webinar.
- P. Zavattieri, J. Youngblood, Nature-Inspired 3D Printing for Sustainable Infrastructure: From Design Concepts to Large-Scale Application, 3D Printing Natural Materials to Unlock Complex Nature-Inspired Infrastructure Collaborative Workshop: Feb 2024, EWN, US Army Corp of Engineers (RDEC).
- Poster, Purdue Civil and Constr. Engineering Research Showcase Sept 12, 20204

7. References

- [1] [Nebraska tests suggest U.S. highways are not ready for widespread EV use | Nebraska Today](#)
- [2] [Nebraska experts weigh highway safety and electric vehicles | Nebraska Today \(unl.edu\)](#)
- [3] [UNL researchers test roadside barriers against heavy EVs in new study |](#)
- [4] [UNL researchers test how electric vehicle crashes can damage road barriers \(1011now.com\)](#)
- [5] <https://www.fischer.senate.gov/public/index.cfm/2024/7/solving-the-hidden-safety-risks-of-evs>
- [6] N. A. Yaraghi *et al.*, “A Sinusoidally Architected Helicoidal Biocomposite,” *Adv. Mater.*, vol. 28, no. 32, pp. 6835–6844, 2016, doi: 10.1002/adma.201600786.
- [7] W. Huang *et al.*, “Multiscale Toughening Mechanisms in Biological Materials and Bioinspired Designs,” *Advanced Materials*, vol. 31, no. 43. Wiley-VCH Verlag, Oct. 01, 2019. doi: 10.1002/adma.201901561.
- [8] S. N. Patek, W. L. Korff, and R. L. Caldwell, “Deadly strike mechanism of a mantis shrimp,” *Nature*, vol. 428, no. 6985, pp. 819–820, 2004, doi: 10.1038/428819a.
- [9] N. Suksangpanya, N. A. Yaraghi, D. Kisailus, and P. Zavattieri, “Twisting cracks in Bouligand structures,” *J. Mech. Behav. Biomed. Mater.*, vol. 76, no. June, pp. 38–57, 2017, doi: 10.1016/j.jmbbm.2017.06.010.
- [10] D. Restrepo, N. D. Mankame, and P. D. Zavattieri, “Phase transforming cellular materials,” *Extrem. Mech. Lett.*, vol. 4, pp. 52–60, 2015, doi: 10.1016/j.eml.2015.08.001.
- [11] M. Thota and K. W. Wang, “Reconfigurable origami sonic barriers with tunable bandgaps for traffic noise mitigation,” no. April 2017, 2024, doi: 10.1063/1.4991026.